ARTICLE

Enhancing the anisole hydrodeoxygenation activity over Ni/Nb_2O_{5-x} by tuning the oxophilicity of the support

Received 00th January 20xx,
Accepted 00th January 20xx

DOI: 10.1039/x0xx00000x

Hadi Ali,[a,b,c] Tom Vandevyvere,[b,d] Jeroen Lauwaert,[d] Sushil Kumar Kansal,[e] Maarten K. Sabbe,[b,d] Shunmugavel Saravanamurugan,*[a] and Joris W.Thybaut*[b]

The present work focuses on designing a robust non-noble metal-based niobia-supported catalyst with a high number of oxygen vacancies for an efficient HDO activity of anisole. Various synthesis procedures, such as hydrothermal (Nb_2O_5-HT), precipitation (Nb_2O_5-P) and hydrolysis (Nb_2O_5-H), are adopted for the preparation of the Nb_2O_5 support, followed by 3wt% Ni impregnation. As a benchmark, Ni has also been impregnated on commercial Nb_2O_5 (Nb_2O_5-C). The catalysts displayed a large discrepancy in surface areas, the crystallite size of Nb_2O_5 and NiOx, strong metal-support interaction (SMSI), active interfacial Ni-NbOx species and oxygen vacancies. Especially, Ni impregnated on Nb_2O_5-H (Ni/Nb_2O_5-H) possesses the highest amount of oxygen vacancies (202 µmol/g) (O_2-temperature programmed desorption), which is 1.1 and 3.5 fold higher than for Ni/Nb_2O_5-HT and Ni/Nb_2O_5-P, respectively, indicating the importance of the synthesis procedure of the support. Interestingly Ni/Nb_2O_5-H has 200-fold higher oxygen vacancies than Ni/Nb_2O_5-C. Likewise, Ni/Nb_2O_5-H possesses a high Ni^{3+}/Ni^{2+} and Nb^{4+}/Nb^{5+} ratio, based on X-ray photoelectron spectroscopy, suggesting high dispersion of small NiOx particles on the NbOx surface, facilitating the redistribution of the electron at the interface of NiO and Nb_2O_5 due to SMSI. This leads to the formation of active interfacial Ni-NbOx species and oxygen vacancies (confirmed by H_2-TPD and XPS), contributing to the activation of hydrogen and anisole adsorption and thereby improving HDO activity substantially. At similar conversions of anisole, Ni/Nb_2O_5-H exhibit the highest rate of HDO of 0.63 $mmol.min^{-1}.g^{-1,}$ which is 1.4 to 3.2 fold higher than other catalysts, including Nb_2O_5-C. Under optimised reaction conditions, Ni/Nb_2O_5-H shows a remarkable activity towards HDO of anisole with an excellent selectivity of cyclohexane (96.5%) at the near-quantitative conversion of anisole (>98%) at 240 °C, 20 bar H_2, 2 h. Ni/Nb_2O_5-H also displays good to excellent activity towards various lignin-based model compounds, affording 50-96% cyclohexane yield.

1. Introduction

Lignocellulosic biomass is an abundant renewable carbon resource that can be directly converted into bio-oil through thermochemical processes such as pyrolysis. Among the constituents of lignocellulosic biomass, lignin is an underutilised phenolic polymer and is mainly produced as waste during the biomass-to-ethanol process in bio-refineries and paper and pulp industries.[1-2] However, after the thermochemical conversion, bio-oil has a high oxygen content (30-50 wt %) in the form of, for example, phenolic compounds, which leads to low fuel efficiency and makes it rather corrosive. Additionally, it is also characterised by high viscosity and poor stability.[3-5] A subsequent deoxygenation step, particularly hydrodeoxygenation (HDO), is crucial for further upgrading the bio-oil. Much attention has been paid to developing heterogeneous catalysts for the direct HDO of lignin and lignin oil for obtaining cycloalkanes.[6-9] Owing to the complex and recalcitrant structure of lignin, various lignin model compounds (e.g., cresol, anisole, guaiacol etc.) have been extensively studied to understand the deoxygenation ability of specific catalysts and gain fundamental insight into the mechanistic pathway of these phenolic compounds.[10-12] Generally, HDO reaction requires a bifunctional catalyst consisting of a metallic site for hydrogenation/dehydrogenation and an oxophillic site for adsorption and activating the oxygen-containing molecule.[12]

Transition metal sulfides, phosphides, carbides and nitrides catalysts have also been employed for the HDO of phenolics.[3, 11–16] However, most of them encounter significant drawbacks, such as poisoning or leaching of catalytic sites, product contamination, deactivation by carbon deposition and lower stability under hydrothermal conditions.[3, 12-14] In line with this, noble metal-based catalysts are widely employed due to their easy H_2 activation and dissociation on the surface of the catalyst to react with other adsorbed reactants. Recently, noble metals (Pt, Pd, and Ru) supported on reducible metal oxides supports (TiO_2, ZrO_2, Nb_2O_5, and CeO_2) exhibited excellent activity toward deoxygenation of phenolics to hydrocarbons compared to catalysts using a non-reducible metal oxide supports (alumina, mesoporous silica and zeolites).[17–20] These results were ascribed to strong metal-support interaction (SMSI). Correspondingly, a wide range of reducible metal oxide supports,

[a] Laboratory of bioproduct Chemistry, Center of Innovative and Applied Bioprocessing, Sector 81 (knowledge City), Mohali-140306, Punjab, India, Email: saravana@ciab.res.in.
[b] Laboratory for Chemical Technology (LCT), Ghent University, Technologiepark 125, 9052, Ghent, Belgium. Email: joris.thybaut@ugent.be
[c] Energy Research Centre, Panjab University, Chandigarh 160014, India
[d] Industrial Catalysis and Adsorption Technology (INCAT), Valentin Vaerwyckweg 1, 9000, Ghent, Belgium
[e] Department of Chemical Engineering and Technology, Panjab University, Chandigarh 160014, India

† Footnotes relating to the title and/or authors should appear here.
Electronic Supplementary Information (ESI) available: [details of any supplementary information available should be included here]. See DOI: 10.1039/x0xx00000x

such as TiO_2, ZrO_2 and CeO_2, have excellent redox characteristics property, robust hydrothermal stability, and much potential for the process related to industrial biomass transformation.[21–23]

Reducible metal oxide supports possess surface oxygen vacancies to adsorb and activate C–O bonds of phenolics and active metal-support interface due to SMSI, contributing to excellent catalytic activity.[12] In line with this, NbOx has also gained much attention due to its high thermal stability and water tolerance.[24] Pt/Nb_2O_5 showed an excellent HDO activity for the deoxygenation of fatty acids and triglycerides to linear alkanes with a yield of 88-100% at 180-250 ^oC, at 8 bar H_2.[25] Likewise, various precious metals (Pt, Pd, or Ru) supported on Nb_2O_5 exhibited a good activity towards HDO of lignin to obtain hydrocarbons (60-71 wt% selectivity) in a temperature range of 250 to 310 ^oC, 5 to 7 bar H_2 pressure for 20 to 40 h.[26–28]. Similarly, Pd/Nb_2O_5 showed 90-99-fold higher catalytic activity and 40-fold higher benzene selectivity during the vapour phase HDO of phenol compared to non-acidic support (Pd/SiO_2) at 300 ^oC.[19, 29] The higher catalytic activity of Pd/Nb_2O_5-based catalysts was achieved due to oxophilic sites formed by the generation of Nb^{4+}/Nb^{5+} near the perimeter (oxophilic sites close to the boundary of metal particles) of metal (Pd) particles.[19] Ru supported on different morphologies of Nb_2O_5 (flower, hollow, mesoporous, and layered) was also studied for the aqueous phase HDO of m-cresol at 250 ^oC, 5 bar H_2 and it was found that layered Nb_2O_5 displayed nearly 90% toluene selectivity with a complete conversion after 3 h.[41] Moreover, the study has been expanded to the deoxygenation of enzymatic lignin, where Ru/Nb_2O_5 showed higher catalytic activity with 99.6% hydrocarbon yield and 94.8% selectivity towards arenes at 250 ^oC, 7 bar H_2 and 20 h. The rationale behind the higher catalytic activity is that it is caused by the presence of more unsaturated niobium oxide (Nb=O) groups and better Ru dispersion revealed by X-ray absorption near edge structure (XANES) and Diffuse Reflectance Infrared Fourier Transform (DRIFTS).[41] The above studies dealt with noble metals (Pt, Pd, Ru), which are relatively expensive due to their limited availability in the earth's crust, provoking the need for non-noble metal-containing HDO catalysts.

A bulk $Ni_{0.9}Nb_{0.1}$ catalyst was developed and explored for the HDO of anisole, resulting in 100% selectivity towards the cyclohexane with the quantitative conversion of anisole at 240 ^oC, 30 bar H_2 after 4 h.[30] Similarly, a highly loaded (15wt% Ni) on Nb_2O_5 showed 100% selectivity towards cyclohexane with 100% conversion of diphenylether at 200 ^oC, 40 bar H_2 pressure for 4 h.[31] Studies on Ni on NbOx support are scarcely reported, and the development of cheaper catalysts based on non-precious metals, such as Ni (with low content), on stable supports, without compromising efficient catalytic activity and selectivity towards deoxygenated products and their stability/recyclability is still challenging for the HDO of phenolics to hydrocarbons.

Generally, niobium oxide exists in various crystalline phases, such as monoclinic, orthorhombic, and pseudohexagonal, with different physicochemical properties related to structural integrity, stability, and acidity, affecting its catalytic activity. Among these crystalline phases, the pseudohexagonal crystalline form of Nb_2O_5 has a greater degree of distortion in the polyhedral structure due to an oxygen-deficient environment where each niobium is adjoined with 4 to 6 oxygen atoms enhancing the possibility of having the highest number of oxygen vacancies, playing a pivotal role in HDO reactions.[32] Based on the above viewpoints, especially the pseudohexagonal phase of Nb_2O_5 having more oxygen vacancies, it has inspired us to synthesise Nb_2O_5 with varied physiochemical characteristic features using precipitation and hydrothermal synthesis approaches. In addition, the prepared supports were impregnated with a low amount of 3wt% non-precious metal Ni, and their catalytic roles were evaluated for the anisole HDO activity and selectivity towards hydrocarbons. Furthermore, the recyclability was assessed as well. The active catalytic species and characteristic features of the synthesised Ni/Nb_2O_5 are pinpointed with the help of basic and advanced characterisation techniques.

2. Experimental Procedures

2.1 Materials

Niobium ethoxide (99.95%), niobium chloride (99.0%), niobium oxide (99.99%), nickel nitrate hexahydrate (99.999%), cyclohexanol (ReagentPlus®, 99%), 2, 6-dimethoxyphenol (99%) and benzene (analytical standard) were supplied from Sigma-Aldrich. Ammonia solution (28% in water), Urea (>99%), anisole (>99.0% GC), catechol (>99% GC), phenol (>99.5% GC), guaiacol (>98.0% GC), guaiacylglycerol-β-guaiacyl ether (97.0% GC), cyclohexane (>99.5% GC), methoxycyclohexane (>98.0% GC), dodecane (>99.0% GC) and decane (>99.0% GC) were supplied from TCI and used as received.

2.2 Catalyst preparation

Nb_2O_5-P supports were synthesised by precipitation method using ammonia solution as a precipitant. Typically, 3 g of $NbCl_5$ was dissolved in 80 mL of ethanol under stirring. The resulting clear solutions were stirred for 1 h, after which precipitant (28% NH_3 in water) was added under vigorous stirring until reaching a pH of ~9. The solution was then stirred for 30 min and aged for 6 h under static conditions at room temperature. Finally, the precipitate was filtered and washed with Milli-Q H_2O until no Cl ions were detected anymore in the filtrate using the $AgNO_3$ solution, followed by drying at 120 ^oC overnight and calcination at 500 ^oC for 5 h with a ramp of 3 ^oC/min under static air. The obtained final product was denoted as Nb_2O_5-P. Likewise, Nb_2O_5-HT was prepared by adopting a hydrothermal approach where 1M aqueous urea was used as a precipitating agent. Typically, 3 g of $NbCl_5$ was dissolved in 80 mL of ethanol, and the resulting clear solution was stirred for 1 h, followed by dropwise addition of 200 mL of 1 M aqueous urea. The solution was stirred for 1 h, and then the whole mixture was transferred into the 500 ml Teflon-lined stainless-steel autoclave and kept at 120 ^oC for 24 h. Afterwards, the same washing procedure mentioned above was followed to obtain Nb_2O_5-HT. Nb_2O_5-H support was synthesised by a hydrolysis method. 6 mL of niobium ethoxide was first taken in a

beaker, followed by adding 10 mL of MilliQ water in a dropwise manner, forming a white precipitate. The resulting precipitate was dried directly in the oven at 120 °C overnight and calcined as mentioned above to obtain Nb_2O_5-H. The various Nb_2O_5 supports were impregnated with 3wt% Ni by the wet impregnation method. The supports (Nb_2O_5-HT, Nb_2O_5-P, Nb_2O_5-H and Nb_2O_5-C) were slowly added into the round bottom flask containing 0.025 M aqueous solution of nickel nitrate hexahydrate. The mixture was stirred for 3 h at ambient temperature. The resulting slurry was evaporated at 110 °C while stirring, dried in an oven at 120 °C overnight and calcined at 450 °C for 4 h with a ramp of 2 °C/min under static air to obtain corresponding 3wt% Ni on the Nb_2O_5 catalysts.

2.3 Catalyst characterisation

The N_2-sorption analysis was carried out in a Quantachrome Autosorb iQ physisorption analyser under liquid nitrogen temperature. Typically, 50 mg catalyst was placed in a 6 mm bulb quartz tube and degassed at 300 °C for 3 h prior to analysis. Brunauer–Emmett–Teller **(**BET) method was used to calculate the surface area, whereas Barrett–Joyner–Halenda (BJH) method was used to determine the pore diameter from the desorption branch. The total pore volume was obtained from the amount of N_2 adsorbed at a relative pressure of about 0.99. The actual amount of Ni present in the catalysts was quantified by (Inductively coupled plasma-mass spectrometry (ICP-MS) using Agilent 7700 and PerkinElmer Nexlon 5000 instrument.

The diffractograms of all the catalysts were collected in the 2θ range of 10-90º at a scan rate of 10º/min using a powder X-ray diffractometer (Rigaku smartlab SE) with x'Celerator solid-state detector with operating parameters of 40 kV, 30 mA and Cu-K (λ = 1.54 Å). The Raman spectra were obtained using a Renishaw Raman Spectrometer equipped with a 514 nm laser. FTIR analyses were conducted using a Perkin Elmer - Spectrum RX-I in the wavenumber range of 450 to 4000 cm^{-1}.

The reduction behaviour of the catalysts was investigated with H_2 temperature-programmed reduction (H_2-TPR) measurement using a BELCAT II chemisorption analyser equipped with a thermal conductivity detector (TCD). In a typical measurement, 20 mg of a catalyst was taken in the quartz tube and reduced from 50 to 800 °C under the flow of 5% H_2/Ar (30 mL/min) with a heating ramp of 10 °C/min, and the employed gas was passed through the molecular sieves trap before reaching the TCD.

X-ray photoelectron spectroscopy (XPS) measurement of the prepared catalysts was carried out in a PHI 5000 Versa Prob II, FEI Inc. (pass setting of 23.5 eV, 0.025eV step, 50ms time per step, and 10 cycles) with a monochromatic Al K X-ray source. The C1s line at 284.5 eV was used to calibrate the binding energies from the adventitious carbon. The UV-Vis spectra were acquired in the wavelength range of 200-600 nm using a Shimadzu 2600 spectrometer in diffuse reflectance mode (DRS-UV-Vis).

O_2-TPD and H_2-TPD analyses were also performed in the same chemisorption analyser used for H_2-TPR. For O_2-TPD, typically, 50 mg of catalyst was placed in a quartz tube and preheated at 200 °C for 1 h under a He flow (50 mL/min) to eliminate moisture; the O_2 was adsorbed by passing 5% O_2/He (50ml/min) at 100 °C for 30 minutes followed by He flow (50 mL/min) to remove physisorbed O_2. Finally, the O_2-TPD was performed using TCD from 100 to 800 °C at a rate of 10 °C/min. For H_2-TPD analysis, 50 mg of catalyst was placed in a quartz tube and reduced at 400 °C for 1 h under a 5.1% H_2/Ar (50 mL/min) followed by cooling down to 50 °C prior to analysis. 5.1% H_2/Ar (50mL/min) at 50 °C was then passed through the catalyst for 30 minutes, followed by Ar (50mL/min) flow for 30 min. Finally, the H_2-TPD measurement was performed using a thermal conductivity detector (TCD) between 50 and 800 °C at a rate of 10 °C/min, and the desorbed gas was passed through molecular sieves before reaching TCD.

2.4 Catalytic performance testing

HDO of anisole was performed in a 50 mL high-pressure Parr reactor. The appropriate amount of substrate, catalyst, dodecane as internal standard and decane as a solvent were placed in a 50 ml stainless steel vessel. The reaction mixture was flushed three times with N_2, followed by three cycles with H_2 before pressuring to the required pressure. The reaction mixture was then heated to the desired temperature and allowed to stir at 450 rpm for a given time. After having reacted, the reaction was stopped by quenching the reactor vessel with ice water. The reaction mixture was filtered off with a 0.2 µm filter, and the sample was then analysed in gas chromatography-mass spectrometry GC-MS (Agilent 7890B) with a flame ionisation detector (FID) detector using a DB-5 MS column. The conversion of the substrate and the yield of products were quantified based on a series of respective individual standards. The conversion, yield, and selectivity of products were calculated as given below.

$$\textbf{Yield}\ (\%) = \frac{\textbf{mol of product produced}}{\textbf{mol of anisole fed}} \times \mathbf{100}$$

$$\textbf{Selectivity}\ (\%) = \frac{\textbf{mol of deoxygenated products}}{\textbf{mol of anisole converted}} \times \mathbf{100}$$

$$\textbf{Conversion}\ (\%) = \frac{\textbf{Initial mol of anisole} - \textbf{Final mol of anisole.}}{\textbf{Initial mol Anisole}} \times \mathbf{100}$$

3. Results and discussion

The various synthesised Ni/Nb_2O_5 catalysts were subjected to different basic and advanced characterisation techniques to understand the structural and physicochemical properties and the catalytically active sites. The well-characterised Ni/Nb_2O_5 catalysts were investigated towards HDO of anisole. This section provides the correlation between the catalytic properties and catalytic activity of Ni/Nb_2O_5 catalysts towards their deoxygenation ability for anisole HDO.

Table 1. Physiochemical properties Ni/Nb_2O_5 catalysts

Entry	Catalysts	Ni (Wt%)[a]	BET (m^2/g)	Pore size (nm)	Pore volume (cm^3/g)	FWHM Nb_2O_5 (100) (degree)	Nb_2O_5 Size (nm)[b]	NiO size (nm)[c]
1	Ni/Nb_2O_5-C	2.97	8(6)	3.4(3.8)	0.03(0.01)	0.180	47.0	NA
2	Ni/Nb_2O_5-P	2.78	9(8)	3.8(3.8)	0.03(0.03)	0.221	38.3	12.1
3	Ni/Nb_2O_5-HT	2.98	47(51)	7.8(7.8)	0.11(0.12)	0.312	27.1	9.5
4	Ni/Nb_2O_5-H	2.73	53(57)	6.5(6.5)	0.27(0.29)	0.367	23.0	7.5

The values in the parenthesis correspond to bare supports. [a] calculated from ICP-MS analysis, [b and c] crystallite size of Nb_2O_5 (100) and NiO (200) based on XRD using the Scherrer equation, respectively.

3.1 Catalyst characterisation

3.1.1 Structural and physicochemical characterisation

The physicochemical properties of bare supports and Ni impregnated on various Nb_2O_5 supports are shown in Table 1. The obtained results revealed that the catalysts possessed varied surface areas, pore sizes and pore volumes due to the different synthesis procedures adopted. The Ni supported on commercial Nb_2O_5 (Nb_2O_5-C) and on the support prepared by the precipitation method (Nb_2O_5-P) exhibited a low surface area of 8 and 9 m^2/g with a small pore size of 3.4 and 3.8 nm, respectively, and negligible pore volume. Interestingly, Ni on the support prepared using the hydrothermal and the hydrolysis methods, Nb_2O_5-HT and Nb_2O_5-H, displayed larger surface areas (47 and 53 m^2/g) and larger pore sizes (7.8 and 6.5 nm) along with increased pore volumes (0.11 and 0.27 cm^3/g), respectively, compared to the other catalysts. However, all the catalysts showed type IV isotherm with different types of the hysteresis loop. Ni/Nb_2O_5-HT possessed a type H1 hysteresis loop, indicating narrow pores size distribution corresponding to mesopores. Ni/Nb_2O_5-H and Ni/Nb_2O_5-P displayed a type H3 hysteresis loop with a wider range of P/P_o, indicating a broad pore size distribution. Ni/Nb_2O_5-C exhibited a tiny hysteresis loop with negligible porosity. (Figure S1).

The XRD diffractogram of Ni/Nb_2O_5 catalysts and bare supports are shown in Figures 1 and Figure S2, respectively. Nb_2O_5-C exhibited the peaks corresponding to the mixture of orthorhombic at 2θ of 22.6, 28.3, 28.9, 36.6, 37.0, 47.5 and 55.1° ascribed to (001), (180), (200), (181), (201), (002) and (182) lattice planes, respectively (JCPDS: 30-0873) and of monoclinic phase at 2θ of 23.8, 24.5, 25.5 and 26.6° attributed to (110), (004), (402) and (111) lattice planes, respectively.[33–34] On the other hand, other Nb_2O_5 supports showed the characteristics peaks assigned to the pseudohexagonal phase at 2θ of 22.5, 28.4, 36.6, 46.1, and 55.1° ascribed to the (001), (100), (101), (002) and (102) lattice planes, respectively (JCPDS: 28-317).[35–36] A NiO diffraction peak can also be seen at a 2θ value of 43.3°, which can be ascribed to the (200) plane for Ni/Nb_2O_5 catalysts (Figure 1).[9, 61] The NiO and Nb_2O_5 crystallite sizes were calculated using the Scherrer equation based on the reflection at 2θ of 22.6 and 43.3°, respectively (Table 1). Interestingly, Ni/Nb_2O_5-H possessed the smallest NiO particle size (7.5 nm), indicating well dispersion of Ni particles over the Nb_2O_5 matrix due to the relatively high surface area and large pore size. Correspondingly, Ni/ Nb_2O_5-P and Ni/Nb_2O_5-HT had relatively bigger NiO particles (9-12 nm), which could be due to their lower surface area, leading to agglomeration.

The peak broadening in the XRD pattern of the catalysts indicated that the synthesis procedure had an effect on the crystalline structure. The crystallite size of Nb_2O_5 in the Ni/Nb_2O_5 catalysts based on the peak detected at 2θ of 28.5° follows the order of Ni/Nb_2O_5-C (47.0 nm)> Ni/ Nb_2O_5-P (38.3 nm) > Ni/Nb_2O_5-HT (27.1 nm)> Ni/ Nb_2O_5-H (23.0 nm). The decrease in the Nb_2O_5 crystallite size can be related to the formation of oxygen vacancies, as in line with the previously reported literature; [38] thus, expecting Ni/ Nb_2O_5-H could possess more oxygen vacancies in its structure.[38]

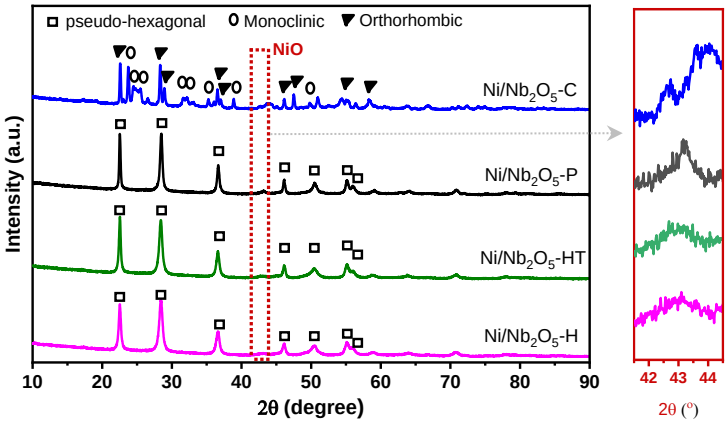

Figure 1. XRD diffractograms of Ni/Nb_2O_5 catalysts

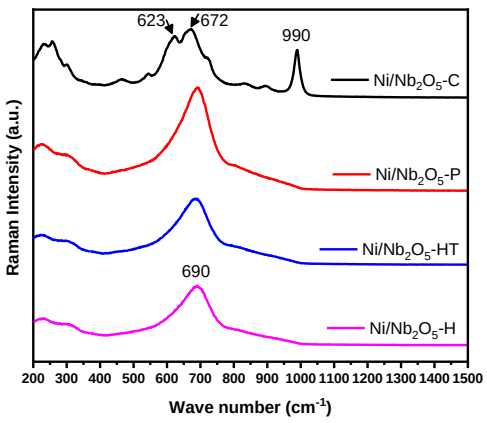

Figure 2. Raman spectra of Ni/Nb_2O_5 catalysts

Raman spectroscopy is a useful technique to determine the bond order of the metal oxides in the region of metal-oxygen stretching modes. Ni/Nb_2O_5-H, Ni/Nb_2O_5-HT and Ni/Nb_2O_5-P displayed a strong Raman broadband at ~690 cm^{-1} (Figure 2), linked to the characteristic vibrations of Nb-O-Nb bridges from a slightly distorted octahedral NbO_6 connected with shared corners.[35] On the contrary, the spectrum of Ni/Nb_2O_5-C exhibited a doublet band at 622 and 673 cm^{-1} and a sharp peak around 990 cm^{-1} attributed to the edge-sharing NbO_6 with many short Nb-O bonds in a closely packed structure.[39–40] The band between 200 and 300 cm^{-1} is attributed to the bending mode of Nb-O-Nb linkages. Similarly, the weak and broad Raman band at ~900 cm^{-1} can be ascribed to the presence of a small amount of unsaturated Nb=O groups (distorted octahedra).[35, 40–41] Moreover, when compared to Ni/Nb_2O_5-P, the peaks of Ni/Nb_2O_5-H and Ni/Nb_2O_5-HT seemed to be broader and less intense, indicating a more deformed structure caused by the presence of more oxygen vacancies.[42–43] The Raman spectrum of Nb_2O_5-C matches well with that of the monoclinic and orthorhombic phases of Nb_2O_5, whereas other Nb_2O_5 supports match well with that of the pseudohexagonal phase of Nb_2O_5, in agreement with the XRD results (Figure 1).[35, 40] FTIR spectra of the Ni/Nb_2O_5 catalysts are shown in Figure S3. No significant difference in the absorption pattern of each catalyst was observed. It can be seen that a broad absorption peak between 3200 and 3600 cm^{-1} and 1618 cm^{-1} appeared, ascribing to the stretching vibration of -OH groups caused by adsorbed H_2O and a surface hydroxyl group, respectively.[44] Further, the peak that appeared at 607 and 893 cm^{-1} can be assigned to the symmetric stretching of Nb-O-Nb and asymmetric stretching of Nb=O bonds, indicating the crystalline nature of Nb_2O_5.[45–46] HR-TEM images of Ni/Nb_2O_5-H show fringe distances of 0.24 and 0.32 nm (Figure S4), corresponding to the exposed (100) and (101) planes of pseudohexagonal Nb_2O_5, respectively, and are in good agreement with XRD analyses (Figure 1).

3.1.2 Reducibility of the Ni/Nb_2O_5 catalysts

The reducibility of Ni/Nb_2O_5 catalysts and the interaction between Ni and the support were investigated using H_2-TPR (Figure 3), and the H_2 consumption is presented in Table S1. Typically, two significant peaks appeared around 400 and 475 °C and, eventually, a small one at 567 °C, indicating the presence of various types of Ni species on the Nb_2O_5 support due to varying metal-support interactions.[47, 61] The peak that appeared around 400 °C can be attributed to the reduction of NiOx to metallic Ni species that weakly interacted with the Nb_2O_5 surface, whereas the peaks that appeared at higher temperatures (around 475 °C and 567 °C) can be ascribed to the NiOx species strongly interacting with the support.[47, 61, 70] Ni/Nb_2O_5-C and Ni/ Nb_2O_5-P showed a significant proportion of NiOx species with weak interaction with Nb_2O_5, which could be correlated with large NiOx particles as in line with XRD results and previous studies.[47, 70] On the other hand, Ni/Nb_2O_5-HT and Ni/Nb_2O_5-H showed relatively lower H_2 consumption at a temperature of 400 °C, suggesting a lower number of larger NiOx particles. At higher temperatures, H_2-consumption was relatively higher, indicating the presence of somewhat smaller NiOx particles strongly interacting with Nb_2O_5.[47, 70] In a nutshell, these findings provide evidence for the presence of a Ni-NbOx interface in Ni/Nb_2O_5-HT and Ni/Nb_2O_5-H promoted by the large surface area and offering a greater number of binding sites for Ni. The DRS-UV-Vis analysis further substantiated the Ni-NbOx interface (Figure S5). Ni/Nb_2O_5-H and Ni/Nb_2O_5-HT showed a relatively higher absorption than Ni/Nb_2O_5-C and Ni/ Nb_2O_5-P in the visible region (λ ~ 450 nm), indicating a strong interaction between NiO and Nb_2O_5 at the interface, leading to the charge transfer from Ni^{2+} to Nb^{5+}, in good agreement with literature.[60]

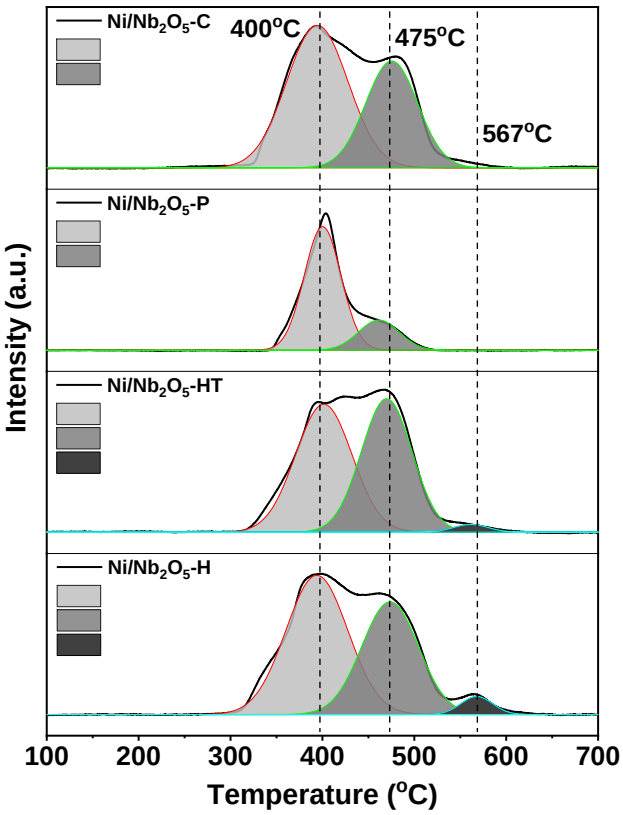

Figure 3. H_2-TPR profile of Ni/Nb_2O_5 catalysts

3.1.3 Surface oxidation species contributing to the catalytic activity

The chemical composition and oxidation states of as-prepared Ni/Nb_2O_5 catalysts were studied with XPS analysis, and the corresponding spectra are shown in Figures 4 and S6. The relative content of different species, such as Ni^{2+}, Ni^{3+}, Nb^{5+}, Nb^{4+}, O_α, O_β and O_γ, were obtained by integrating the area under the particular curve

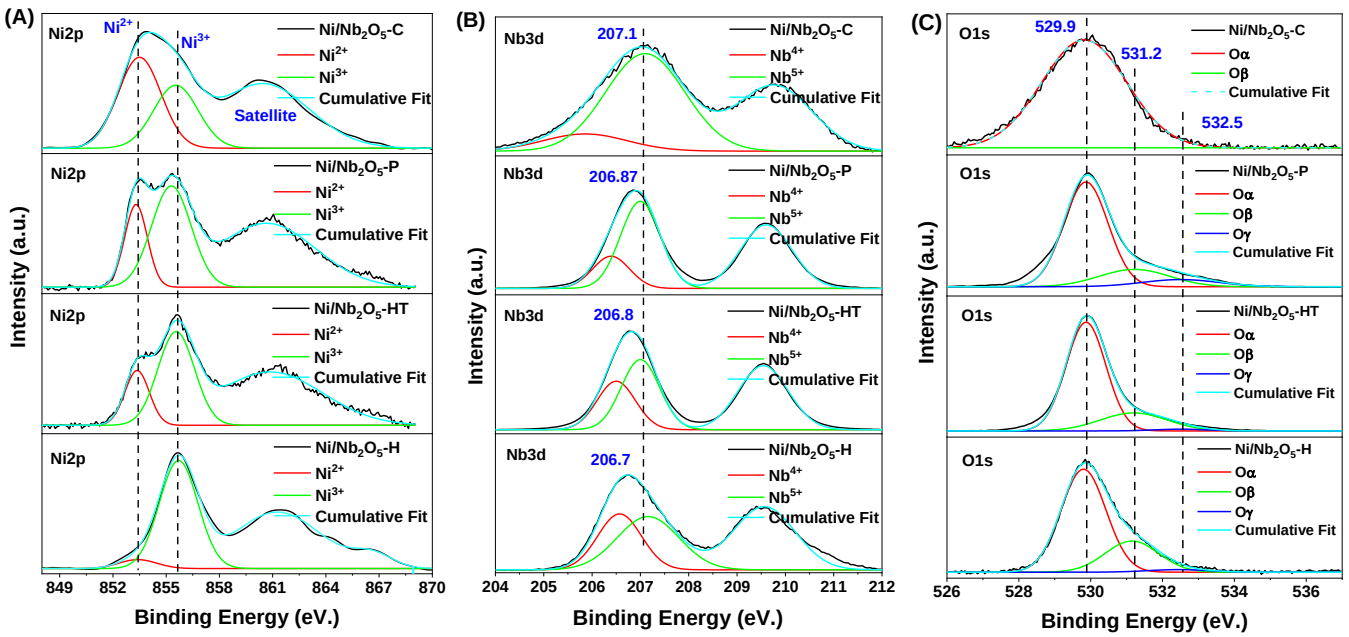

Figure 4. XPS spectra of (A) Ni2p, (B) Nb3d and (C) O1s of Ni/Nb_2O_5 catalysts

after deconvolution of the corresponding raw XPS data (Table 2). Figure (4a) shows the XPS spectra of $Ni2p_{3/2}$ with a major peak at 853.5 and 855.7 eV for all Ni/Nb_2O_5 catalysts after deconvolution, attributed to Ni^{2+} and Ni^{3+} species on the surface, respectively.[48–49] In addition, a satellite peak at 861.7 eV was also observed. It can be noted that the ratio of Ni^{3+}/Ni^{2+} increase in the order of Ni/Nb_2O_5-C < Ni/Nb_2O_5-P < Ni/Nb_2O_5-HT < Ni/Nb_2O_5-H (Table 2 and Figure 4a). The highest fraction of Ni^{3+} in the Ni/Nb_2O_5-H was observed, which could be correlated with a high dispersion of small NiOx particles on the NbOx surface, resulting in the electron redistribution at the interface of NiOx and Nb_2O_5 due to SMSI, complementarily creating defects (i.e., Nb^{4+}).[50–51] Ni/Nb_2O_5-C displays spin-orbit doublets with a binding energy of 207.1 and 209.8 eV corresponding to $Nb3d_{5/2}$ and $Nb3d_{3/2}$ (Figure 4b), suggesting the existence of a fully oxidised form of Nb^{5+}.[39, 52] Impressively, Ni/Nb_2O_5-P, Ni/Nb_2O_5-HT and Ni/Nb_2O_5-H exhibited a shift towards lower binding energy in the decreasing order of 206.87, 206.8 and 206.7 eV, respectively, indicating the changes in the chemical environment around Nb due to lattice deformation and the formation of oxygen vacancies as in line with the XRD and Raman results.[35, 53] Further, the formation of oxygen vacancies caused by the generation of more Nb^{4+} species character in the Nb_2O_5 network results in a peak shift towards lower binding energy, as in good agreement with the previously reported study.[35]

Moreover, the $Nb3d_{5/2}$ spectra of Ni/Nb_2O_5 showed peaks at binding energy values of 207.1 and 205.8-206.6 eV after deconvolution, corresponding to Nb^{5+} and Nb^{4+}, respectively, as in good accordance with previous reports.[35] Interestingly, the relative ratio of Nb^{4+}/Nb^{5+} for Ni/Nb_2O_5-H was found to be the highest (0.75), which is more than four-fold higher than what was obtained for Ni/Nb_2O_5-C (0.19) (Table 2). The O1s XPS spectra further substantiated the formation of oxygen vacancies by comparing Ni/Nb_2O_5-C and Ni/Nb_2O_5-H (Figure 4c). The O1s spectra of Ni/Nb_2O_5-C exhibited a single peak at 529.9 eV after deconvolution corresponding to lattice oxygen, whereas other catalysts displayed three peaks at 529.8, 531.2 and 532.5 eV attributed to lattice oxygen (Oα), oxygen vacancies (Oβ) and surface hydroxyl (Oγ), respectively.[54–55] When considering the density of oxygen vacancies in a catalyst, it is noteworthy to mention that the Oβ species increased in the order of Ni/Nb_2O_5-P < Ni/Nb_2O_5-HT < Ni/Nb_2O_5-H, depending upon Nb_2O_5 synthesis approach as in line with the ratio of Nb^{4+}/Nb^{5+} (Figure 4c and Table 2). Having significant oxygen vacancies aids in the preferential adsorption of the oxygen moiety of anisole on these sites, making deoxygenation more likely.[35]

XPS spectra of Ni/Nb_2O_5-C and Ni/Nb_2O_5-H after reduction at 400 °C for 1 h were also measured, as shown in Figure S6. The $Ni2p_{3/2}$ spectra of the catalysts exhibited the peak binding energy corresponding to metallic Ni (851.6 eV). However, both unreduced Ni^{2+} (in the case of Ni/Nb_2O_5-C) and Ni^{3+} existed on the surface, and it was obvious that not all of the NiOx had been reduced at 400 °C as in accordance with the H_2-TPR. During the reduction process, the hydrogen spillover from the metallic Ni surface facilitates the formation of partially reduced Nb_2O_{5-x} due to SMSI, consequently enhancing the oxygen vacancies near the metal-support interface, playing an essential role in the catalytic HDO activity as per the earlier studies.[25, 49, 54, 56] Moreover, the Nb3d spectrum of Ni/Nb_2O_5-H showed a lower binding energy shift of 206.7 to 206.4 eV compared to Ni/Nb_2O_5-C (207.1 to 206.8 eV), respectively, suggesting the formation of more oxygen vacancies (representing Nb^{4+}) in the presence of Ni upon reduction at 400 °C.[57] With regard to this, the ratio of O_β/O_{total} was calculated and found to be increasing from 0 to 0.24 and 0.26 to 0.35 after reducing Ni/Nb_2O_5-C and Ni/Nb_2O_5-H, respectively (Table 2 and S1), corroborating the enhancement of oxygen vacancies during the reduction process. However, the intensity of Ni $2p_{3/2}$ significantly decreased after reduction, inferring

Table 2. XPS and O_2-TPD results of Ni/Nb_2O_5 catalysts.

Catalysts	Ni $2p_{3/2}$	Nb $3d_{5/2}$		O 1s	O_2 (µmol/g) [a]
	Ni^{3+}/Ni^{2+}	Nb^{4+}/Nb^{5+}	Nb^{4+}/Nb^{4+}+ Nb^{5+}	O_β/ O_{total}	
Ni/Nb_2O_5-C	0.71	0.19	0.16	0.00	1
Ni/Nb_2O_5-P	2.14	0.34	0.25	0.19	58
Ni/Nb_2O_5-HT	2.55	0.69	0.41	0.22	189
Ni/Nb_2O_5-H	12.43	0.75	0.43	0.26	202

[a] Amount of O_2- desorption derived from O_2-TPD

the decreased exposure of metallic Ni on the surface of the NbOx network due to possible passivation of metallic Ni by reducible NbOx.[49, 54]

3.1.4 Chemisorption measurements: Characteristic features of Ni/Nb_2O_5 contributing to the catalytic activity

To further investigate the occurrence of oxygen vacancies, an O_2-TPD analysis of all Ni/Nb_2O_5 catalysts was performed, and corresponding profiles are shown in Figure 5. It is known that the O_2 species desorbed below <250 °C and between 250-400 °C belong to physically and chemically adsorbed oxygen species on the catalyst surface, respectively, often represented as oxygen vacancies.[58] The desorption peak between 400 and 600 °C is attributed to the sub-surface lattice oxygen, and the one above 600 °C desorbed oxygen corresponds to lattice oxygen.[58–59] It can be seen that Ni/Nb_2O_5-H and Ni/Nb_2O_5-HT exhibited a major peak at T_{max} of 323 °C in addition to a small and broad peak at 174 ℃ compared to the Ni/Nb_2O_5-C and Ni/Nb_2O_5-P. Another small and broad peak appeared at T_{max} of 607 °C, ascribed to the evolution of lattice oxygen. The amount of desorbed oxygen species below 400 °C follows the order of Ni/Nb_2O_5-H (202 µmol/g) > Ni/Nb_2O_5-HT (189 µmol/g) > Ni/ Nb_2O_5-P (58 µmol/g) > Ni/Nb_2O_5-C (1µmol/g) (Table 2), suggesting Ni/Nb_2O_5-H possessing the highest amount of oxygen vacancies as in line with the XPS analysis.

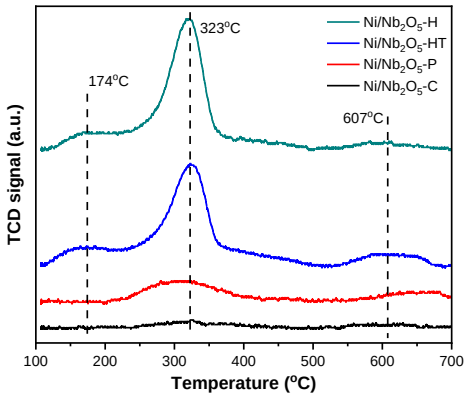

Figure 5. O_2-TPD profile of Ni/Nb_2O_5 catalysts

H_2-TPD was employed to identify various types of metal sites and quantify the amount of hydrogen adsorbed on the sites of the Ni/Nb_2O_5 catalysts (Table S1 and Figure 6). The peak that appears >300 °C could be ascribed to hydrogen spillover from the support or hydrogen that is strongly adsorbed on the Ni sites, contributing to inferior activity towards HDO.[37, 47, 55, 61–62] In contrast, the low-temperature peak emerging below 200 °C can be attributed to hydrogen species that weakly interact on the surface of bigger Ni crystallites. [47, 55, 63] Such a significant peak was observed in the case of Ni/Nb_2O_5-C, followed by a small intensity for other catalysts with an order of Ni/ Nb_2O_5-P > Ni/Nb_2O_5-HT ≈ Ni/Nb_2O_5-H as in line with the XRD results. The peak that appeared between 200 and 300 °C (medium temperature) can be associated with active hydrogen species adsorbed on the perimeter sites of small nickel crystallites at the interface between the nickel and the Nb_2O_5 support.[37, 47, 64]

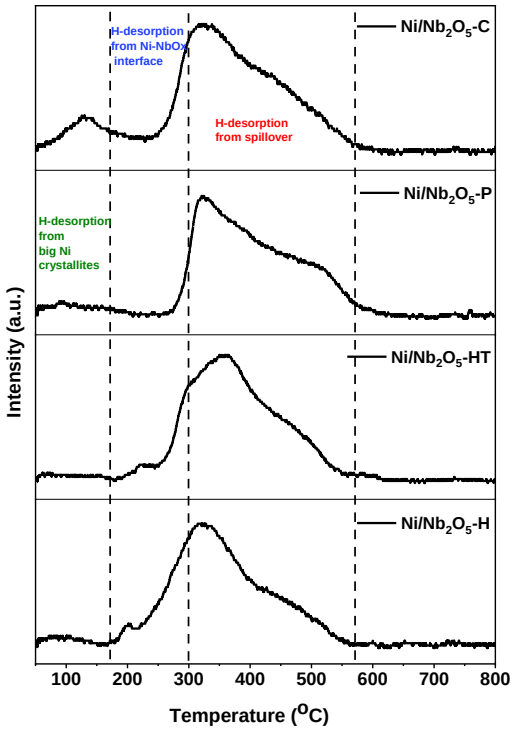

Figure 6. H_2-TPD of Ni/Nb_2O_5 catalysts

Ni/Nb_2O_5-H (5.5µmol/g; 24%) showed a prominent peak, followed by other catalysts in the order of Ni/Nb_2O_5-HT (4.2 µmol/g; 14%) > Ni/Nb_2O_5-C (3.4 µmol/g; 13%) > Ni/ Nb_2O_5-P (1.0 µmol/g; 4%) (Table S1), expecting to be catalytically active for the HDO reaction as observed in the previous study. [37]

3.2 Catalytic performance

3.2.1 Screening of Ni/Nb_2O_5 catalysts

The catalytic performance of various Nb_2O_5 supported Ni catalysts was investigated for the HDO of anisole under identical conditions (Figure 7). Ni/Nb_2O_5-C and Ni/Nb_2O_5-P exhibited the highest anisole conversion of ~58% among the tested catalysts. Irrespective of such significant conversion, Ni/Nb_2O_5-C and Ni/Nb_2O_5-P showed comparatively low selectivity of 21 and 35% towards deoxygenated (DeO) products (cyclohexane and benzene), respectively. The higher conversion and low selectivity over these two catalysts could be attributed to the presence of large NiOx particles and low density of oxygen vacancies, as evident by XRD and XPS results, respectively (Figures 1 and 4). The large size of NiOx particles in Ni/Nb_2O_5-C and Ni/Nb_2O_5-P was considered accountable for the adsorption of anisole through its aromatic ring, predominantly favouring the ring hydrogenation of anisole to produce methoxycyclohexane (selectivity; 51 and 39%), respectively. Then, demethylation of the formed methoxycyclohexane occurred, giving 24.6 and 19% selectivity towards cyclohexanol with the respective catalyst. These results are in line with the previously reported studies related to HDO of phenolic.[17, 65] The deoxygenation ability of Ni/Nb_2O_5-P was 1.5-fold higher than Ni/Nb_2O_5-C in terms of selectivity (35.4%) towards cyclohexane and benzene. This activity discrepancy can be correlated with the presence of a higher amount of oxygen vacancies in Ni/Nb_2O_5-P as compared to Ni/Nb_2O_5-C, as is evident from the O_2-TPD and XPS analysis (Table 2).

Intriguingly, Ni/Nb_2O_5-H and Ni/Nb_2O_5-HT exhibited the highest selectivity of ~44% towards DeO products (cyclohexane and benzene) under identical reaction conditions (Figure 7). This can be ascribed to the higher amount of oxygen vacancies and active H species formed on the perimeter of the smaller NiOx particle, as revealed by XPS, O_2-TPD and H_2-TPD analysis (Table 2, Figures 4 and 5). Such vacancies exhibit a strong interaction with the oxygen moiety of anisole (C_{Ar}-O), leading to the activation of the C–O bond and active metal sites provide the necessary H species for HDO at the metal-support interface, resulting in an easier cleavage of anisole's C_{Ar}-O bond.[55,67] The greater selectivity towards DeO products (cyclohexane and benzene) indicates direct deoxygenation as the possible predominant pathway for HDO of anisole over these catalysts. Though a higher selectivity of DeO products was achieved with Ni/Nb_2O_5-H and Ni/Nb_2O_5-HT, the interface of Ni (small particles) (Table 1) and NbOx in the SMSI state is responsible for lowering the conversion at the low reaction temperature (200 °C), as in good accordance with the previous study.[66] Further, the smaller size of NiOx particles can be facilitated by the large surface area of Nb_2O_5-HT and Nb_2O_5-H, depending upon the catalyst preparation method.

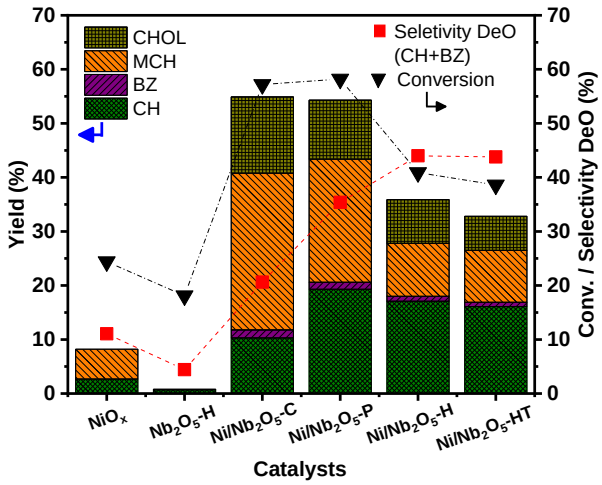

Figure 7. HDO of anisole with Ni/Nb_2O_5 catalysts (Reaction conditions: 100 mg catalysts, 2 mmol anisole, 20 g decane, 200 ºC, 40 bar H_2, 450 rpm, 1 h. All the catalysts were reduced with formier gas (5% H_2 in N_2) at 400 °C for 1 h prior to the reaction. CHOL (cyclohexanol), MCH (methoxycyclohexane), BZ (benzene), CH(cyclohexane), DeO (deoxygenated products; benzene and cyclohexane).

3.2.2 Selectivity of deoxygenated products at similar conversion

Comparing the catalysts activity at a similar conversion allows for an objective evaluation of the selectivity between the catalysts. To that end, Ni/Nb_2O_5 catalysts were examined at similar conversions of anisole (30-45%) to see their catalytic efficiency in terms of deoxygenation ability. The product distribution and the rate of formation of HDO products (R_{HDO}) (cyclohexane and benzene) from anisole are tabulated in Table 3. Ni/Nb_2O_5-HT exhibited the highest selectivity towards the deoxygenated products (77.3%), with the lowest rate of formation of DeO products with R_{HDO} of 0.20 mmol. min^{-1} g^{-1}. This indicates that Ni/Nb_2O_5-HT possesses SMSI as confirmed by H_2-TPR analysis, as a consequence of which a significant part of the NiOx does not get reduced during the prereduction treatment. This causes an adverse impact by decreasing the amount of potential active sites since it is expected that NiOx itself does not exhibit catalytic activity.

Interestingly, Ni/Nb_2O_5-H displayed relatively high selectivity towards DeO products (69.5%) with the highest rate of formation of DeO products, R_{HDO} (0.63 mmol. min^{-1} g^{-1}), which is three-fold higher than Ni/Nb_2O_5-HT. The rationale behind the enhanced HDO activity of Ni/Nb_2O_5-H was due to the abundance of active hydrogen species adsorbed on the perimeter sites of small nickel crystallites at the interface between the nickel and Nb_2O_5 support as compared to other Ni/Nb_2O_5 catalysts as observed in H_2-TPD measurements (Figure 6, Table S1). Moreover, Ni/Nb_2O_5-H possessed more active metallic sites, unlike Ni/Nb_2O_5-HT (based on H_2-TPR and H_2-TPD) and higher oxygen vacancies according to the O1s spectra of XPS (Figure 4c). In addition to the above viewpoints, the presence of a large pore size might have also enhanced the accessibility of oxygen vacancies for the substrate and thus contributed to the improved catalytic activity for anisole HDO.

Table 3. Product distributions and rate of formation of HDO products at similar conversion

Catalysts	Time (min.)	Conv. (%)	Sel. DeO (%)	Product distribution (%)				R_{HDO} (mmol. min^{-1}. g^{-1})
				CH	BZ	MCH	CHOL	
Ni/ Nb_2O_5-C	15	46.0	36.3	14.1	2.6	15.2	10.0	0.45
Ni/ Nb_2O_5-P	15	33.5	42.4	11.3	2.9	9.7	5.8	0.38
Ni/ Nb_2O_5-HT	45	29.5	77.3	20.5	2.3	2.9	0.8	0.20
Ni/Nb_2O_5-H	15	34.1	69.5	21.2	2.5	4.7	2.4	0.63

Reaction conditions: 50 mg catalysts, 2 mmol anisole, 20 g decane, 20 bar H_2, 240 °C, 450 rpm. All the catalysts were reduced with formier gas (5%H_2 in N_2) at 400 °C for 1h prior to the reaction.
Rate of HDO (R_{HDO}) = (mmol)DeO/catalyst mass* time

For comparison, Ni/Nb_2O_5-C was also studied at a similar conversion and displayed the lowest selectivity towards DeO products (36.3%) with a moderate R_{HDO} (0.45 mmol. min^{-1} g^{-1}) which is 1.4 times lower than Ni/Nb_2O_5-H. O_2-TPD and XPS (Figure 4, 5 and table 2) analyses indicate that Ni/Nb_2O_5-C had a relatively lower amount of oxygen vacancies than Ni/Nb_2O_5-H, emphasising the importance of these defect sites in enhancing the deoxygenation activity. Similarly, Ni/Nb_2O_5-P has moderate catalytic activity in terms of R_{HDO} (Table 3) as compared to Ni/Nb_2O_5-H due to the lower number of oxygen vacancies and lacking metal-support interface, as per O_2-TPD, XPS analysis, H_2-TPD and TPR. These findings indicate the importance of the synthesis procedure of Nb_2O_5 supports since a higher number of oxygen vacancies introduced by the synthesis procedure enhances the catalytic activity for HDO. In a nutshell, the presence of Ni-H species particularly formed at the interface and the nature of metal-support interaction leads to the formation of interfacial Ni-NbOx along with neighbouring oxygen vacancies from Nb_2O_{5-x}, playing a considerable role in the catalytic performance towards the formation of DeO products.

3.2.3 Effect of the reduction temperature

H_2-TPR profiles of Ni/Nb_2O_5 catalysts (Figure 3) indicated that most NiOx species could not be reduced to active Ni^0 at 400 °C during the prereduction step prior to the reaction. Therefore, the effect of prereduction temperature on the best catalyst Ni/Nb_2O_5-H was also investigated. The results indicate that the conversion of anisole decreased from 46 to 34%, with no significant change in the selectivity of DeO products (cyclohexane and benzene) when increasing the reduction temperature from 400 to 500 °C (Figure 8). The decrease in the activity at higher prereduction temperatures might be attributed to the strong metal-support interaction (SMSI), consequently forming a reduced layer of NbOx species on the surface of Ni particles.[49] A similar trend was also observed in a previous study related to the HDO of phenol with Pd/Nb_2O_5. Pd/Nb_2O_5, reduced at 500 °C, displayed significantly lower catalytic activity than Pd/Nb_2O_5 reduced at 300 °C due to complete coverage of Pd nanoparticles by partially reduced NbOx.[19] To get insight into the reduced species, Ni/Nb_2O_5-H, prereduced at 300-500 °C, was subjected to H_2-TPD analysis (Figure S7).

The H_2-TPD profiles indicated that when increasing the reduction temperature from 300 to 400 °C, the total chemisorbed hydrogen progressively increased from 13 to 22 µmol/g, reflected in the anisole conversion increased from 11 to 46% with no change in the product selectivity (Figure 8). This suggests the formation of a greater amount of nickel hydride (Ni-H) species near the perimeter sites of Ni-NbOx (Figure 6, Figure S7) due to the increased generation of active Ni^0 sites, facilitating the dissociation of molecular hydrogen.[55] Consequently, chemisorbed hydrogen increased (as discussed in the H_2-TPD section), leading to higher HDO activity. Moreover, it is known that Ni-H species generated on metallic Ni particles play a significant role in the HDO reaction as a necessary intermediate for hydrogenation.[63] Further, XPS analysis of Ni/Nb_2O_5-H, reduced at 400 °C, also revealed that the formation of oxygen vacancy (O_β/O_{total}) increased to 0.35 from 0.26 (parent Ni/Nb_2O_5-H) (Table 2 and Table S2) due to the partial reduction of Nb_2O_5 to Nb_2O_{5-x} in the proximity of metal (Ni) particle. As a result, the metal-support interface increased due to SMSI, which could be responsible for the higher HDO activity. However, if the prereduction temperature further increased to 500 °C, the chemisorbed H_2 consumption decreased to 15 µmol/g along with a shift of the desorbed H_2 to high temperature (Figure S7), indicating that the number of active H_2 species decreased due to the formation of a reducible NbOx layer over the Ni, leading to less exposed active Ni^0 species for H_2 dissociation.[68] These findings revealed the decrease in the active H_2 species as the reduction temperature increased to 500 °C, leading to lower HDO activity in line with the previously reported literature. [54, 69]

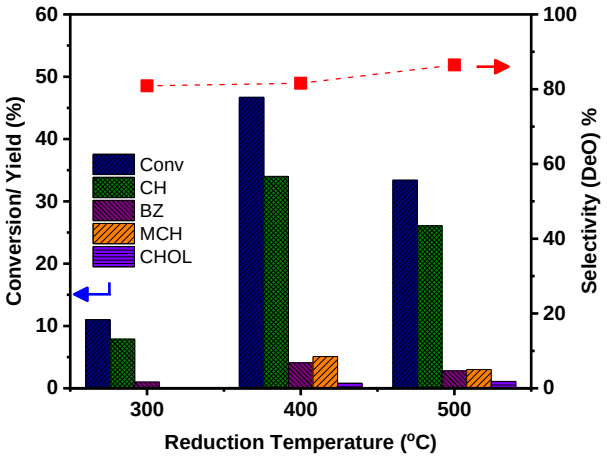

Figure 8. Effect of reduction temperature on the catalytic activity of Ni/Nb_2O_5-H catalyst (Reaction conditions: 50 mg catalyst, 2 mmol anisole, 20 g decane, 40 ºC, 20 bar H_2, 450 rpm, 1 h. Ni/Nb_2O_5-H was reduced with formier gas (5% H_2 in N_2) at different temperatures for 1 h prior to the reaction.

3.2.4 Reaction condition effects and reaction mechanism elucidation

The effects of the other reaction parameters, such as temperature, pressure, reaction time and intermediates as substrate, were also assessed over the best catalyst: Ni/Nb_2O_5-H. Increasing the reaction temperature from 210 to 240 °C, the conversion of anisole increased from 51.9 to 89.9 %, and the DeO products selectivity (cyclohexane and benzene) enhanced from 73 to 91%, respectively, inferring that the higher reaction temperature improved deoxygenation activity (Figure 9A). Concurrently, the yields of methoxycyclohexane and cyclohexanol were below 10 % even at relatively low reaction temperature (210 °C), indicating that the demethoxylation of anisole was the predominant pathway. As the reaction temperature increased from 210 to 240 °C, methoxycyclohexane and cyclohexanol yields decreased from 8.4 to 2.7% and 4.1 to 0.6%, respectively.

The study was expanded further with Ni/Nb_2O_5-H to investigate the effect of pressure at optimised temperature (240 °C) and time (1h) (Figure 9B). The results indicate that at high hydrogen pressure (40 bar), Ni/Nb_2O_5 partially promoted aromatic ring hydrogenation of anisole, giving methoxycyclohexane (5.6%) along with a low yield of benzene (1.4%). This can be attributed to the presence of a higher concentration of active hydrogen species over the Ni^0 sites.[55, 70] Reducing H_2 pressure up to 20 bar, the benzene yields slightly increased to 4.1% while maintaining a similar selectivity towards DeO products (91.0–94.2 %) and conversion (~90%), implying that the H_2 pressure has a small impact on the product selectivity. However, a low yield of methoxycyclohexane (2.7%) was observed at 20 bar H_2 pressure. Interestingly, when reducing H_2 pressure further to 10 bar, the benzene yield increased to 7.2 % with almost unchanged selectivity towards DeO products (85%), manifesting that a low hydrogen pressure hampers the hydrogenation of the aromatic ring, thereby increasing the benzene yield. However, the conversion of anisole decreased to 48.4 % with a low pressure of H_2 (10 bar).

The conversion and product distribution as a function of time over Ni/Nb_2O_5-H are shown in Figure 10. The conversion of anisole after 30 min of reaction was 81.5%, with 88.2% selectivity towards DeO products, i.e., cyclohexane (83.2%) and benzene (5%), indicating high deoxygenation activity. When further increasing the reaction time to 2 h, the conversion of anisole increased to near-quantitative (98.9 %) with an excellent selectivity to DeO products (96.5%, including 3.2% benzene). At the same time, a small fraction of methoxycyclohexane (<4.0%) was observed in 30 min by aromatic hydrogenation of anisole at high hydrogen pressure, which subsequently transformed to cyclohexane for a longer reaction time (2 h) via demethylation and demethoxylation over Ni/Nb_2O_5-H. The results obtained from the various parameters reflected that a small proportion (<8 %) of cyclohexanol and methoxycyclohexane was observed in the reaction mixture, indicating that the direct demethoxylation (DMO) of anisole was faster than the hydrogenation (HYD) of anisole. Overall, Ni/Nb_2O_5-H showed excellent catalytic activity and displayed a 1.1 to 45.0-time higher rate of formation of HDO product (cyclohexane) compared to the previous studies on anisole HDO (Table S3).

Based on obtained results with Ni/Nb_2O_5-H under various reaction conditions, a reaction pathway for the anisole HDO was proposed (Scheme 1). The formation of phenol during anisole HDO was not observed in the reaction products in this study, even at low temperatures and shorter reaction time, suggesting that the reaction proceeds predominantly through the direct demethoxylation of anisole (DMO pathway) followed by the hydrogenation (HYD) of benzene to form cyclohexane. Specifically, the methoxy group of anisole strongly interacts with the oxygen vacancies of Nb_2O_5 and activates the C_{Ar}-O bond with the active hydrogen species over the metal (Ni^0) sites, consequently cleaving the C_{Ar}-O bond to yield benzene.[26, 29] Eventually, cyclohexane is formed by fast hydrogenation of benzene due to the high hydrogenation ability of Ni induced by higher hydrogen pressure. Further, to substantiate the reaction pathway, experiments with the intermediates as substrates, such as methoxycyclohexane, anisole, cyclohexanol, benzene and cyclohexane, were performed (Table 4). Ni/Nb_2O_5-H presented an 18.4% cyclohexane yield when employing methoxycyclohexane as a substrate (25.8% conversion).

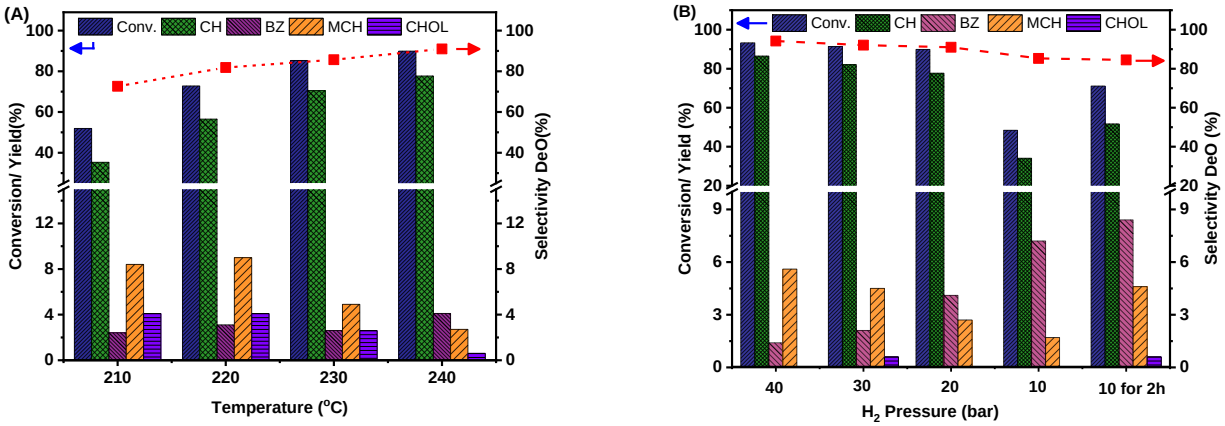

Figure 9. Effect of reaction temperature (A) and Pressure (B) on the catalytic activity of Ni/Nb_2O_5-H catalyst. Reaction conditions: 100 mg catalyst, 2 mmol anisole, 20 g decane; 20 bar (For temperature study), 1 h, 450 rpm. Ni/Nb_2O_5-H was reduced with formier gas (5%H_2 in N_2) at 400 °C for 1 h prior to the reaction.

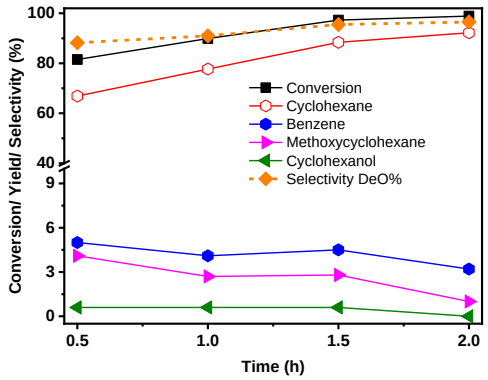

Figure 10. Effect of reaction time on the catalytic activity of Ni/Nb_2O_5-H catalyst. Reaction conditions: 100 mg catalyst, 2 mmol anisole, 20 g decane, 240 ºC, 20 bar H_2, 450 rpm. Ni/Nb_2O_5-H was reduced with formier gas (5% H_2 in N_2) at 400 °C for 1 h prior to the reaction.

On the contrary, when anisole was used as a substrate, the conversion and the yield of DeO products was two-fold higher (46.7 and 38.1%, respectively) under similar reaction condition, suggesting that the rate of direct demethoxylation (DMO) of anisole is much faster rather than the hydrogenation of anisole to methoxycyclohexane with Ni/Nb_2O_5-H. Interestingly, cyclohexanol is inclined to convert completely to cyclohexane, indicating a stronger dehydroxylation ability of Ni/Nb_2O_5-H and reflecting that the cyclohexanol formed during anisole HDO can easily convert to cyclohexane. When employing benzene as a substrate, 71% of benzene was converted to cyclohexane, indicating fast aromatic ring hydrogenation. Almost no conversion occurred when cyclohexane was used as a reactant, indicating that cyclohexane was relatively stable under the reaction conditions. These results demonstrate that the anisole HDO predominantly undergoes direct DMO to yield benzene, which subsequently quickly transforms to cyclohexane under the investigated reaction conditions.

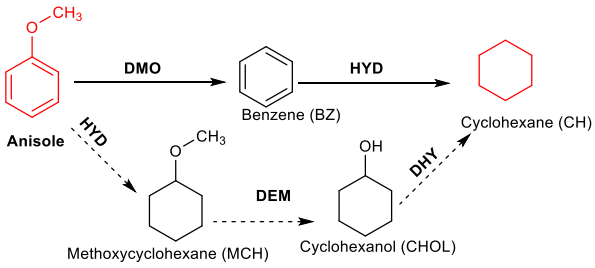

Scheme 1: Plausible mechanism for HDO of anisole

3.2.5 Recyclability of Ni/Nb_2O_5-H catalyst

The reusability of Ni/Nb_2O_5-H was studied at an intermediate anisole conversion (~30%) (Figure 11). After each run, the spent Ni/Nb_2O_5-H catalyst was washed with acetone, air-dried at 120 °C, and then calcined at 450 °C for 4 h before reduction, with formier gas (5% H_2 in N_2) at 400 °C for 1 h. The anisole conversion was 30.9 %, with a DeO products yield of 27.6% under given reaction conditions after the first run. In the subsequent runs, the DeO products yield was

Table 4. Stability and reactivity of substrate and intermediates

Substrate	Conv. (%)	Selec. (DeO)%	Product distribution (yield%)			
			CH	BZ	MCH	CHOL
Anisole	46.7	81.6	34.0	4.1	5.1	0.8
MCH	25.8	73.6	18.4	0.6	-	0.2
CHOL	100.0	92.8	92.1	0.7	0.0	-
Benzene	71.0	-	66.3	-	0	0
cyclohexane	<1.0	-	-	0.2	0	0

Reaction conditions: 50 mg Ni/Nb_2O_5-H, 2 mmol anisole, 20 g decane, 240 ºC, 1 h, 20 bar H_2, 450 rpm. Ni/Nb_2O_5-H was reduced with formier gas (5% H_2 in N_2) at 400 °C for 1 h prior to the reaction.

maintained (~25%) until the fourth run. In contrast, the conversion of anisole slightly increased from 30.9 (first run) to 35.9 (fourth run). The XRD pattern of the spent Ni/Nb_2O_5-H after the fourth run exhibited detectable NiOx species compared to the fresh one (Figure S8), implying NiOx formation caused by the sintering of metal particles, thus leading to a loss of the metal-support interface and resulting in a slight decrease in selectivity.[56]

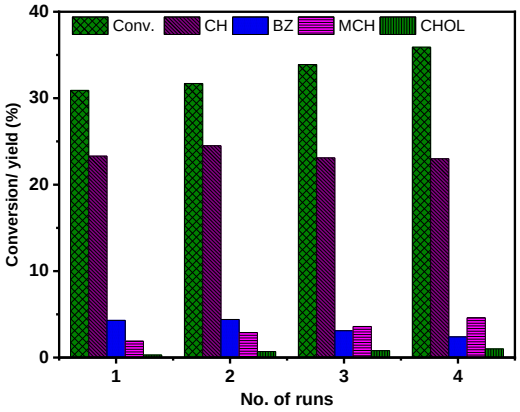

Figure 11. The recyclability of Ni/Nb_2O_5-H catalyst for anisole HDO. Reaction conditions: $m_{cat:\ anisole}$ = 1:4.3, 20 g decane, 240 ºC, 20 min, 20 bar H_2, 450 rpm.

4. Hydrodeoxygenation of various lignin-based substrates

Examining the HDO activity of Ni/Nb_2O_5-H has been expanded to other lignin-based monomers (phenol, catechol, guaiacol, 2,6 dimethoxyphenol; 2, 6-DMP) and dimer (guaiacyl glycerol β-guaicyl ether; GGE) (Table 5). Cyclohexane was formed as the major product from all the substrates. The substrates containing one or two oxygen moieties (phenol, catechol and guaiacol) required a shorter reaction time to obtain an excellent cyclohexane yield (82-96%) (Table 5, entry 1-3) than three oxygen moieties (2, 6 DMP), which needed 10 h reaction time to get about 50% cyclohexane yield (Table 5, entry 4). Moreover, Ni/Nb_2O_5-H showed comparable activity compared to previous reports related to HDO of p-cresol with noble metals (Pt, Pd and Ru) supported on Nb_2O_5.[26,27] One of the most intriguing common lignin-based β-O-4 model compounds, GGE, was also investigated with Ni/Nb_2O_5-H and found to yield deoxygenated products of cyclohexane (64%) and propyl cyclohexane (76%). Furthermore, Ni/Nb_2O_5-H showed excellent activity for the HDO of anisole

Table 5. Hydrodeoxygenation of other monomers and β-O-4 lignin dimer over Ni/Nb_2O_5-H[a]

Entry	Substrate	Conv. (%)	Time (h)	Cyclohexane (yield%)
1	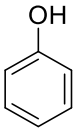	>99	1	**96**
2	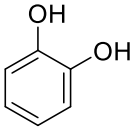	>99	2	**85**
3	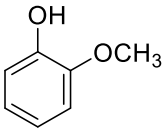	97	2	**82**
4	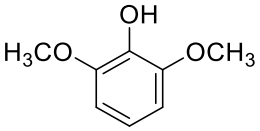	90	10	**49**
[b]5	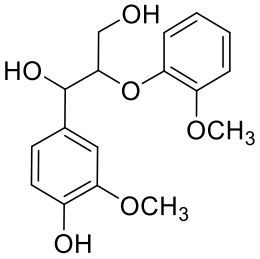	NA	5	**64**[c]

[a]Reaction conditions: [a]100 mg Ni/Nb_2O_5-H, 2 mmol Substrate, 20 g decane, 240 °C, 40 bar H_2, 450 rpm. Ni/Nb_2O_5-H was reduced with formier gas (5% H_2 in N_2) at 400 °C for 1 h prior to the reaction. [b] 50mg GGE and 100 mg Ni/Nb_2O_5-H; [c] 76% of propyl-cyclohexane was also formed (calculated based on assuming 1 mole of GGE gives one mole of cyclohexane and one mole propyl cyclohexane).

compared to previously reported Ni-based catalysts where 10-90 wt% of Ni was employed.[30, 55, 70] This signifies the importance of designing non-noble metal (Ni) supported on reducible metal oxides, paving the way towards exploring the HDO of a wide range of lignin-based oxygenated compounds.

5. Conclusions

We have demonstrated that Nb_2O_5-H, prepared via a hydrolysis approach, possesses a higher surface area that helps limit the size of NiOx particles deposited by impregnation. A relatively small Nb_2O_5 particle, substantiated by XRD, in Ni/Nb_2O_5-H causes a structural distortion of octahedral NbO_6, confirmed by Raman spectroscopy. This leads to the formation of a relatively large amount of oxygen vacancies, corroborated by O_2-TPD and XPS, than other catalysts, including Ni impregnated on commercial Nb_2O_5 (Ni/Nb_2O_5-C). In a nutshell, Ni/Nb_2O_5-H with a high number of oxygen vacancies significantly favours preferential adsorption of anisole towards deoxygenation. The SMSI, confirmed by H_2-TPR, in Ni/Nb_2O_5-H promotes the formation of active interfacial Ni-NbOx species, validated by H_2-TPD and XPS analysis. The presence of active interfacial Ni-NbOx species and a high number of oxygen vacancies- contributing to the activation of H_2 and anisole adsorption, respectively- in Ni-Nb_2O_5-H leads to remarkable anisole HDO activity, yielding an excellent selectivity towards DeO product, cyclohexane (96.5%), with the quantitative conversion of anisole. Ni-Nb_2O_5-H exhibits good catalytic activity with various lignin-based model compounds employed in this study, paving the way towards designing non-noble metal (Ni) supported on reducible metal oxides towards the upgradation of lignin bio-oil.

Conflicts of interest

There are no conflicts to declare.

Acknowledgements

H. A. and S. S. would like to thank the Center of Innovative and Applied Bioprocessing (CIAB), Mohali infrastructural facilities,

for conducting R & D activities. H. A. gratefully thank the Council of Scientific & Industrial Research (CSIR), Government of India, for offering a Senior Research Fellowship (CSIR-SRF) and Energy Research Centre, Panjab University, for PhD registration. H. A. and J. W. T. would like to thank the ERC consolidator grant (i-CaD) and EC (GA no 615456) for financial support while working at LCT. T. V. and J. L. would like to thank the Research Foundation - Flanders (FWO) for the financial support (grant numbers: 3S042419 and 12Z2218N).

References

1 Q. Bu, H. Lei, A. H. Zacher, L. Wang, S. Ren, J. Liang, Y. Wei, Y. Liu, J. Tang, Q. Zhang and R. Ruan, *Bioresour. Technol.*, 2012, **124**, 470-477.

2 M. P. Pandey and C. S. Kim, *Chem. Eng. Technol.*, 2011, **34**, 29-41.

3 M. Saidi, F. Samimi, D. Karimipourfard, T. Nimmanwudipong, B. C. Gates and M. R. Rahimpour, *Energy Environ. Sci.*, 2014, **7**, 103-129.

4 A. Corma, S. Iborra and A. Velty, *Chem. Rev.*, 2007, **107**, 2411-2502.

5 P. M. Mortensen, J. D. Grunwaldt, P. A. Jensen and A. D. Jensen, *ACS Catal.*, 2013, **3**, 1774-1785.

6 X. Li, B. Zhang, X. Pan, J. Ji, Y. Ren, H. Wang, N. Ji, Q. Liu and C. Li, *ChemSusChem*, 2020, ***13***, 4409-4419.

7 S. Gundekari and S. Kumar Karmee, *ChemistrySelect*, 2021, ***6***, 1715-1733.

8 M. Zhao, J. Hu, P. Lu, S. Wu, C. Liu, and Y. Sun, *Fuel*, 2022, ***326***, 125020.

9 H. Ali, S. K. Kansal, and S. Saravanamurugan, In *Biomass, Biofuels, Biochemicals*, 2022, 287-308.

10 C. Ranga, R. Lødeng, V. I. Alexiadis, T. Rajkhowa, H. Bjørkan, S. Chytil, I. H. Svenum, J. Walmsley, C. Detavernier, H. Poelman, P. V. D. Voort and J. W. Thybaut, *Chem. Eng. J.*, 2018, **335**, 120-132.

11 K. Wu, X. Li, W. Wang, Y. Huang, Q. Jiang, W. Li, Y. Chen, Y. Yang, C. Li, *ACS Catal.,* 2021, **12**, 8-17.

12 X. Wang, M. Arai, Q. Wu, C. Zhang and F. Zhao, Green Chem., 2020, **22**, 8140-8168.

13 Z. Jia, N. Ji, X. Diao, X. Li, Y. Zhao, X. Lu, Q. Liu, C. Liu, G. Chen, L. Ma and S. Wang, *ACS Catal.,* 2022, **12**, 1338-1356.

14 A. R. Gollakota, M. Reddy, M. D. Subramanyam and N. Kishore, Renew. Sustain. Energy Rev., 2016, **58**, 1543-1568.

15 K. Wu, W. Wang, H. Guo, Y. Yang, Y. Huang, W. Li, and C. Li, ACS energy letters, 2020, **5**, 1330-1336.

16 X. Diao, N. Ji, X. Li, Y. Rong, Y. Zhao, X. Lu, C. Song, C. Liu, G. Chen, L. Ma, and S. Wang, *Appl. Catal. B: Environ.*, 2022, **305**, 121067.

17 C. Newman, X. Zhou, B. Goundie, I. T. Ghampson, R. A. Pollock, Z. Ross, M. C. Wheeler, R. W. Meulenberg, R. N. Austin and B. G. Frederick, *Appl. Catal. A: Gen.*, 2014, **477**, 64-74.

18 P. M. de Souza, R. C. Rabelo-Neto, L. E. Borges, G. Jacobs, B. H. Davis, D. E. Resasco and F. B. Noronha, *ACS Catal.*, 2017, **7**, 2058-2073.

19 A. M. Barrios, C. A. Teles, P. M. de Souza, R. C. Rabelo-Neto, G. Jacobs, B. H. Davis, L. E. P. Borges and F. B. Noronha, *Catal. Today,* 2018, **302**, 115-124.

20 M. B. Griffin, G. A. Ferguson, D. A. Ruddy, M. J. Biddy, G. T. Beckham and J. A. Schaidle, *ACS Catal.*, 2016, **6**, 2715-2727.

21 P. Sudarsanam, H. Li and T. V. Sagar, *ACS Catal.*, 2020, **10**, 9555-9584.

22 C. A. Teles, R. C. Rabelo-Neto, G. Jacobs, B. H. Davis, D. E. Resasco and F. B. Noronha, *ChemCatChem*, 2017, **9**, 2850-2863.

23 L. Lei, Y. Wang, Z. Zhang, J. An and F. Wang, *ACS Catal.*, 2020, **10**, 8788-8814.

24 W. Guan, X. Chen, S. Jin, C. Li, C. W. Tsang and C. Liang, *Ind. Eng. Chem. Res.*, 2017, **56**, 14034-14042.

25 K. Kon, W. Onodera, S. Takakusagi and K. I. Shimizu, *Catal. Sci. Technol.*, 2014, **4**, 3705-3712.

26 Y. Shao, Q. Xia, L. Dong, X. Liu, X. Han, S. F. Parker, Y. Cheng, L. L. Daemen, A. J. Ramirez-Cuesta, S. Yang and Y. Wang, *Nat. Commun.*, 2017, **8**, 1-9.

27 L. Dong, Y. Shao, X. Han, X. Liu, Q. Xia, S. F. Parker, Y. Cheng, L. L. Daemen, A. J. Ramirez-Cuesta, Y. Wang and S. Yang, *Catal. Sci. Technol.*, 2018, **8**, 6129-6136.

28 L. Dong, L. Lin, X. Han, X. Si, X. Liu, Y. Guo, F. Lu, S. Rudić, S. F. Parker, S. Yang and Y. Wang, *Chem*, 2019, **5**, 1521-1536.

29 C. A. Teles, P. M. de Souza, R. C. Rabelo-Neto, M. B. Griffin, C. Mukarakate, K. A. Orton, D. E. Resasco and F. B. Noronha, *Appl. Catal. B: Environ.*, 2018, **238**, 38-50.

30 J. Xu, P. Zhu, I. H. El Azab, B. B. Xu, Z. Guo, A. Y. Elnaggar, G. A. Mersal, X. Liu, Y. Zhi, Z. Lin and H. Algadi, *Chin. J. Chem. Eng.*, 2022, **49**, 187-197.

31 G. F. Leal, S. Lima, I. Graçe, H. Carrer, D. H. Barrett, E. Teixeira-Neto, A. A. S. Curvelo, C. B. Rodella and R. Rinaldi, *Iscience*, 2019, **15**, 467-488.

32 R. A. Rani, A. S. Zoolfakar, A. P. O'Mullane, M. W. Austin and K. Kalantar-Zadeh, *J. Mater. Chem. A.*, 2014, **2**, 15683-15703.

33 Z. Yu, X. Lü, S. Xun, M. He, L. Zhu, H. Chen, M. Yuan, L. Fan and W. Zhu, *Fuel*, 2022, **307**, 121877.

34 W. Jiang, J. P. Cao, C. Zhu, T. Xie, X. Y. Zhao, M. Zhao, Y. P. Zhao and H. C. Bai, *Fuel*, 2021, **295**, 120635.

35 Y. Wang, S. Aghamohammadi, D. Li, K. Li and R. Farrauto, *Appl. Catal. B: Environ.*, 2019, **244**, 438-447.

36 Y. Zou, Y. Hu, A. Uhrich, Z. Shen, B. Peng, Z. Ji, M. Muhler, G. Zhao, X. Wang and X. Xu, *Appl. Catal. B: Environ.*, 2021, **298**, 120584.

37 Z. He, M. Hu and X. Wang, *Catal. Today*, 2018, **302**, 136-145.

38 S. B. T. Tran, H. Choi, S. Oh and J. Y. Park, *J. Catal.*, 2019, **375**, 124-134.

39 H. T. Kreissl, M. M. Li, Y. K. Peng, K. Nakagawa, T. J. Hooper, J. V. Hanna, A. Shepherd, T. S. Wu, Y. L. Soo, and S. C. E. Tsang, *J. Am. Chem. Soc.*, 2017, **139**, 12670-12680.

40 J. M. Jehng and I. E. Wachs, *Chem. Mater.*, 1991, **3**, 100-107.

41 Y. Xin, L. Dong, Y. Guo, X. Liu, Y. Hu and Y. Wang, *J. Catal.*, 2019, **375**, 202-212.

42 H. Cui, G. Zhu, Y. Xie, W. Zhao, C. Yang, T. Lin, H. Gu and F. Huang, *J. Mater. Chem. A*, 2015, **3**, 11830-11837.

43 W. Zhao, W. Zhao, G. Zhu, T. Lin, F. Xu, and F. Huang, *Dalton Trans.*, 2016, **45**, 3888-3894.

44 Y. Tao, B. Singh, V. Jindal, Z. Tang, and P. P. Pescarmona, *Green Chem.*, 2019, **21**, 5852-5864.

45 P. Nagaraju, R. Vasudevan, A. Alsalme, A. Alghamdi, M. Arivanandhan, and R. Jayavel, *Nanomaterials*, 2020, **10**, 160.

46 A. G. Prado, L. B. Bolzon, C. P. Pedroso, A. O. Moura, and L. L. Costa, Appl. Catal. B: Environ., 2008, **82**, 219-224.

47 D. Messou, V. Bernardin, F. Meunier, M. B. Ordoño, A. Urakawa, B. F. Machado, V. Collière, R. Philippe, P. Serp and C. Le Berre, *J. Catal.*, 2021, **398**, 14-28.

48 O. S. Jeon, H. Lee, K. S. Lee, V. K. Paidi, Y. Ji, O. C. Kwon, J. P. Kim, J. H. Myung, S. Y. Park, Y. J. Yoo, J. G. Lee, S. Y. Lee and Y. G. Shul, *ACS Appl. Mater. Interfaces.*, 2022, **14**, 12140-12148.

49 K. A. Resende, A. H. Braga, F. B. Noronha, and C. E. Hori, *Appl. Catal. B: Environ.*, 2019, **245**, 100-113.

50 K. Raju, S. Rajendran, T. K. Hoang, D. Durgalakshmi, J. Qin, D. E. Diaz-Droguett, F. Gracia, and M. A. Gracia-Pinilla, *J. Power Sources*, 2020, **466**, 228305.

51 S. Ni, H. Qu, H. Xing, Z. Xu, X. Zhu, M. Yuan, L. Wang, J. Yu, Y. Li, L. Yang and H. Liu, *ACS Appl. Mater. Interfaces.* 2021, **13**, 17501-17510.

52 W. Song, Y. He, S. Lai, W. Lai, X. Yi, W. Yang and X. Jiang, *Green Chem.,* 2020, **22**, 1662-1670.
53 Ö. D. Coşkun, S. Demirel and G. Atak, *J. Alloys Compd.*, 2015, **648**, 994-1004.
54 X. Zhao, X. Wu, H. Wang, J. Han, Q. Ge, and X. Zhu, *ChemistrySelect*, 2018, **3**, 10364-10370.
55 Y. Zhang, G. Fan, Y. Lin, L. Yang and F. Li, *Appl. Catal. A: Gen.*, 2022, **631**, 118481.
56 C. A. Teles, R. C. Rabelo-Neto, N. Duong, J. Quiroz, P. H. C. Camargo, G. Jacobs, D. E. Resasco and F. B. Noronha, *Appl. Catal. B: Environ.*, 2020, **277**, 119238.
57 R. Wojcieszak, A. Jasik, S. Monteverdi, M. Ziolek and M. M. Bettahar, *J. Mol. Catal. A: Chem.*, 2006, *256*, 225-233.
58 Y. Wei, Y. Zhang, Y. Chen, F. Wang, Y. Cao, W. Guan and X. Li, *ChemSusChem*, 2022, **15**, e202101983.
59 W. Hong, M. Shao, T. Zhu, H. Wang, Y. Sun, F. Shen and X. Li, *Appl. Catal. B: Environ.*, 2020, **274**, 119088.
60 S. A. Rawool, M. R. Pai, A. M. Banerjee, A. Arya, R. S. Ningthoujam, R. Tewari, R. Rao, B. Chalke, P. Ayyub, A. K. Tripathia and S. R. Bharadwaj, *Appl. Catal. B: Environ.*, 2018, **221**, 443-458.
61 K. V. Chary, K. S. Lakshmi, P. V. R. Rao, K. S. R. Rao and M. Papadaki, *J. Mol. Catal. A: Chem.*, 2004, **223**, 353-361.
62 M. Keane, *Phys. Chem. Chem. Phys.*, 1999, **1**, 3173-3181.
63 P. Yan, J. Mensah, A. Adesina, E. Kennedy and M. Stockenhuber, *Appl. Catal. B: Environ.*, 2020, **267**, 118690.
64 P. Braos-García, C. García-Sancho, A. Infantes-Molina, E. Rodríguez-Castellón and A. Jiménez-López, *Appl. Catal. A: Gen.*, 2010, **381**, 132-144.
65 H. Vargas-Villagran, M. A. Flores-Villeda, I. Puente-Lee, D. A. Solis-Casados, A. Gomez-Cortes, G. Diaz-Guerrero and T. E. Klimova, *Catal. Today*, 2020, **349**, 26-41.
66 Y. Yang, C. Ochoa-Hernández, A. Víctor, P. Pizarro, J. M. Coronado, D. P. Serrano, *Appl. Catal. B: Environ.,* 2014, **145**, 91-100.
67 H. Ali, T. Vandevyvere, J. Lauwaert, S. K. Kansal, S. Saravanamurugan and J. W. Thybaut, *Catal. Commun.*, 2022, **164**, 106436.
68 L. F. de Sousa, F. S. Toniolo, S. M. Landi and M. Schmal, *Appl. Catal. A: Gen.*, 2017, **537**, 100-110.
69 K. A. Resende, F. B. Noronha and C. E. Hori, *Renew. Energy*, 2020, **149**, 198-207.
70 S. Jin, Z. Xiao, Li, C., X. Chen, L. Wang, J. Xing, W. Li and C. Liang, *Catal. Today*, 2014, **234**, 125-132.

Table of content (TOC)

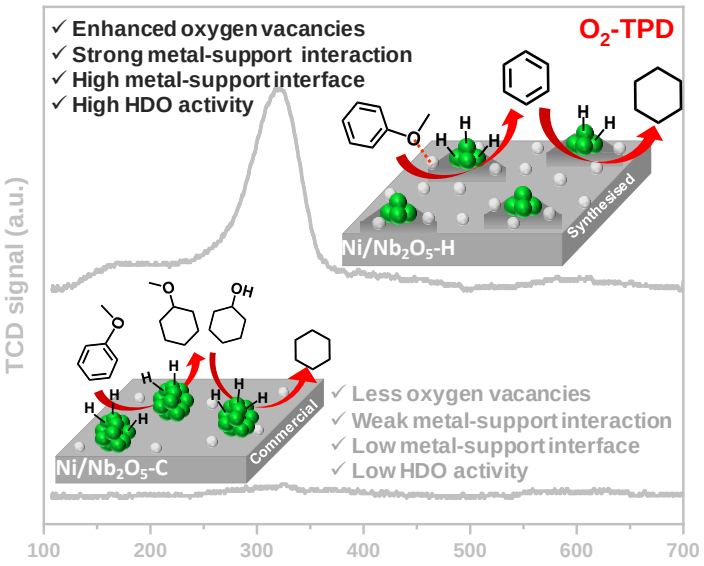

Ni impregnated on Nb_2O_5-H, prepared via the hydrolysis method, (Ni/Nb_2O_5-H) possesses a higher number of oxygen vacancies and metal-support interface than Ni impregnated on commercial Nb_2O_5 (Ni/Nb_2O_5-C), resulting in enhanced selectivity towards deoxygenated products under identical reaction conditions.